Journal of Computational Physics **180,** 339–357 (2002)
doi:10.1006/jcph.2002.7098

A Critical Comparison of Eulerian-Grid-Based Vlasov Solvers

T. D. Arber and R. G. L. Vann

Physics Department, University Warwick, Coventry, CV4 7AL, United Kingdom
E-mail: tda@astro.warwick.ac.uk

Received January 19, 2002; revised April 23, 2002; published online June 19, 2002

A common problem with direct Vlasov solvers is ensuring that the distribution function remains positive. A related problem is to guarantee that the numerical scheme does not introduce false oscillations in velocity space. In this paper we use a variety of schemes to assess the importance of these issues and to determine an optimal strategy for Eulerian split approaches to Vlasov solvers. From these tests we conclude that maintaining positivity is less important than correctly dissipating the fine-scale structure which arises naturally in the solution to many Vlasov problems. Furthermore we show that there are distinct advantages to using high-order schemes, i.e., third order rather than second. A natural choice which satisfies all of these requirements is the piecewise parabolic method (PPM), which is applied here to Vlasov's equation for the first time.

Key Words: Vlasov.

1. INTRODUCTION

A considerable amount of effort in plasma physics is devoted to the elucidation and exploitation of fundamental kinetic processes. Such studies usually require a detailed calculation of the particle distribution function $f(\mathbf{r}, \mathbf{v}, t)$, where $(\mathbf{r}, \mathbf{v})$ are the position and velocity vectors, respectively. For many nonlinear processes this calculation can only be performed numerically. There are two equally important numerical approaches to this problem.

Particle-in-cell (PIC) methods approximate the plasma by a finite number of macroparticles which move in the self-consistent fields computed by taking moments on a background mesh. The key drawback with this approach is that the numerical noise only decreases as $1/\sqrt{N}$, where N is the number of macroparticles in any particular computational cell. This problem is particularly pronounced in studies where the fine-scale structure of $f(\mathbf{r}, \mathbf{v}, t)$ is important or where the physics of interest is in the high-energy tail of the distribution in which there is only a relatively small fraction of the total number of macroparticles. Even

0021-9991/02 $35.00

with these limitations the PIC approach continues to produce accurate results when the high-energy tail is not significant, and a sufficiently high N can be maintained to resolve the broad distribution function. Recent examples of the application of PIC methods range from studies of laser plasma scattering [1] to simulations of the lunar wake [2].

This paper deals with an alternative to the PIC approach based on solving Vlasov's equation for $f(\mathbf{r}, \mathbf{v}, t)$, along with Maxwell's equations, directly. We restrict our examples to one spatial and velocity dimension and zero magnetic field. Such 1D problems can only satisfy Maxwell's equations if there is zero net current in the system. In some of the examples below, and commonly in the literature, we ignore this restriction, as it does not affect the validity of the numerical comparisons. We consider only two species—ions and electrons, say, with opposite charges of equal magnitude and mass ratio $m_i/m_e = M_r$ The Vlasov equation becomes

$$\partial_t f_e + v\partial_x f_e - E\partial_v f_e = 0, \tag{1}$$

$$\partial_t f_i + v\partial_x f_i + \frac{1}{M_r} E\partial_v f_i = 0, \tag{2}$$

where E is $|q_e|/m_e$ times the electric field. We solve either Poisson's equation

$$\partial_x E = W \int (f_i - f_e)\, dv \tag{3}$$

or Ampère's equation

$$\partial_t E = -W \int v(f_i - f_e)\, dv \tag{4}$$

for the electric field. We set the physical parameter $W = q_e^2/m_e\epsilon_0$ to unity. This is consistent with a normalization of spatial lengths to the Debye length (λ_D), velocities to the thermal speed (v_{the}), time to λ_D/v_{the}, and E to $m_e v_{the}^2/e\lambda_D$, where $\lambda_D^2 = \epsilon_0 k_B T_e/n_0 e^2$, $v_{the}^2 = k_B T_e/m_e$, and n_0 is the equilibrium number density. We can consider the motion of the electrons only (valid in the limit M_r large) by treating the ions as a stationary and uniform background.

Throughout this paper we restrict our attention to split Eulerian schemes. This technique rests on splitting the Vlasov solver into separate spatial and velocity space updates and has the advantage that each of these updates can then be treated as simple advections at constant speed. Since the original, ground-breaking publication [3] most attention on fixed-grid Vlasov solvers has concentrated on improving the accuracy of the advection sweeps. Recent examples have included use of MacCormack's method [4] and conservative schemes [5]. A common problem with all Vlasov solvers is that the solutions to Vlasov's equation often involve a fine-scale filamentation which increases in time. For example the solution to the linear Landau damping problem has a perturbed distribution function which varies as $\exp(ikvt)$. Higher order schemes have a tendency to produce Gibbs overshoot when this occurs unless some additional averaging is applied. A related problem is that there is no guarantee, except for first-order schemes, that the numerical solution has not introduced regions of negative distribution function. Both of these problems are identical to the problems encountered in the treatment of shocks in computational fluid mechanics. Ways of avoiding the restrictions imposed on the order of the scheme by Godunov's theorem in fluid dynamics have a direct analogy in the solution of Vlasov problems. In this paper

we concentrate on studying the importance of positivity, order, and monotonicity in the advection steps by comparing a variety of codes with different properties.

Previous work on the direct solution of Vlasov's equation has also made use of spectral methods, e.g. [6], and semi-Lagrangian methods, e.g. [7]. In this article we restrict attention to grids in the physical x and v coordinates, but note briefly that these methods suffer the same problems as high (>1st)-order unlimited Eulerian schemes. A positivity-preserving, or monotonicity-preserving, spectral scheme has yet to be developed. In this paper the only attempt towards spectral accuracy is through tests of high-order compact schemes.

The rest of the paper is organized as follows. In the next section we describe each of the test codes in detail. This is followed by the results for the three test problems chosen. Next we consider the viability of using Ampère's law, instead of Poisson's equation, to solve for the electric field. Finally we discuss these results and outline the conclusions which can be drawn from these tests.

2. THE CODES

All of the codes solve for the distribution function f on a fixed Eulerian grid with grid spacings $(\Delta x, \Delta v)$ in spatial and velocity coordinates, respectively. All codes use the same time-splitting algorithm and the same FFT solver for the electric field. Thus the only differences between the schemes are in the implementation of the advection steps in the x and v directions. In this way all differences in accuracy can be attributed to the different advection schemes alone. We have not compared these results with PIC codes, semi-Lagrangian Vlasov solvers, or spectral Vlasov solvers. The aim throughout has been to determine the best fixed Eulerian grid advection scheme for Vlasov problems. Attention is also restricted to 1D problems, i.e., one spatial dimension and one velocity dimension, but there is no reason why these schemes cannot be generalized to multidimensional problems.

The common time-stepping algorithm is as follows:

- Evolve $\partial_t f + v\partial_x f = 0$ for a time $\Delta t/2$.
- Solve Poisson's equation for the electric field.
- Evolve $\partial_t f + E\partial_v f = 0$ for a time Δt (noting that this does not change E).
- Finally, evolve $\partial_t f + v\partial_x f = 0$ for a time $\Delta t/2$.

This splitting is second order in time and has the advantage that each of the x or v updates is a linear advection with constant speed, i.e., solves an equation of the form

$$\partial_t U + c\partial_x U = 0, \tag{5}$$

where c is not a function of U or x.

The numerical problem is therefore reduced to finding an accurate, and fast, constant speed advection solver. This is clearly not a new problem in computational physics! What is new is how well classical advection solvers perform when applied to the Vlasov equation with its alternating x and v advections coupled through a self-consistent field.

Recall that, thinking of U as a fluid density, the evolution of the advection equation (5) for a time Δt is simply a uniform shift of the fluid by a displacement $c\,\Delta t$. Our problem is that we know U only at a set of discrete grid points $\{x_j = j\,\Delta x\}$. There are two particular properties that we hope to find in an advection solver.

(a) The method should not introduce false extrema (which is equivalent to it preserving monotonicity), i.e., requiring that if, for $0 < \lambda < 1$, $U_{i-1}^n < U_i^n < U_{i+1}^n$, then $U_i^{n+1} \le U_{i+1}^{n+1}$ (and similarly for monotone decreasing), where $\lambda = c\Delta t/\Delta x$.

(b) The method should not accentuate already existing extrema, i.e., for $0 < \lambda < 1$, if $U_{i-1}^n < U_i^n > U_{i+1}^n$, then $U_i^n \ge \max\{U_i^{n+1}, U_{i+1}^{n+1}\}$ (and similarly for minima).

Properties (a) and (b) together imply the method is positivity preserving and total variation diminishing (TVD).

One solution would be to spline interpolate between the grid points by some function $\tilde{U}(y)$ and write $U(y_i, t + \Delta t) = \tilde{U}(y_i - \lambda, t)$, where $y = x/\Delta x$ (so $y_i = i$) and λ is the distance in y by which the fluid must be shifted. However, by a corollary of Godunov's theorem, any interpolation scheme that is higher than first order breaks properties (a, b).

In this paper we consider a number of schemes, all of which are cast in conservative form. They work in the following way:

- At any time t^n, we consider $U_i^n = U(y_i, t^n)$ to be the amount of fluid in the cell $i - 1/2 < y < i + 1/2$.
- Using the $\{U_j\}$, we construct a function $\phi(y)$ to represent the amount of fluid at each point y. Note that ϕ need not be continuous everywhere.
- Compute the amount of fluid flowing (in the positive direction) through the boundary between the ith cell and the $(i + 1)$th cell,

$$\Phi_{i+1/2} = \int_{i+1/2-\lambda}^{i+1/2} \phi(y)\, dy. \tag{6}$$

- Evolve the system by one time step:

$$U_i^{n+1} = U_i^n - \left(\Phi_{i+1/2} - \Phi_{i-1/2}\right). \tag{7}$$

In all cases the time step, Δt, is limited so that $\Delta t = MIN(\Delta x/v^{\max}, \Delta v/|E|_{\max})$, where $v^{\max}$ is the largest velocity allowed on the grid and $|E|_{\max}$ is the maximum value of the absolute magnitude of the electric field.

2.1. Flux Balance Method (FB)

The first advection solver to be considered is the flux balance method (FB). The interpolation function $\phi(y)$ is piecewise linear and is discontinuous at cell boundaries:

$$D_i = (U_{i+1} - U_{i-1})/2, \tag{8}$$

$$\phi(y) = U_i + D_i y, \quad y \in [i - 1/2, i + 1/2]. \tag{9}$$

This then defines a trapezium, through the midpoint of the cell with the specified gradient, bounded in x by the cell boundaries. U_i is then updated via Eq. (7). $\Phi_{i+1/2}$ is the flux through the right-hand-side boundary determined from the area of the trapezium which would be advected through this boundary when moved at constant speed c. There are several problems with this approach: it is only second-order accurate in space and there is no guarantee that it either preserves monotonicity or does not introduce false extrema. When coupled with smoothing and averaging techniques, to dissipate fine-scale structure, this approach has been shown to be successful for a variety of Vlasov problems [8].

2.2. Van Leer-Limited Scheme (VL)

To obtain what we hereafter refer to as the VL method, we adapt the FB method as follows:

- Estimate of the gradient from a third-order upwind scheme [9].
- Apply the following van Leer gradient limiter to the gradients D_i before calculating the cell boundary fluxes $F_{i+1/2}$,

$$D_i = s \min(|D_i|\Delta x, 2|U_{i+1} - U_i|, 2|U_i - U_{i-1}|),$$

where

$$\begin{aligned} s &= \text{sign}(U_{i+1} - U_i) \quad && \text{if } \text{sign}(U_{i+1} - U_i) = \text{sign}(U_i - U_{i-1}), \\ s &= 0 && \text{otherwise.} \end{aligned}$$

- Compute ϕ as in Eq. (9).

Note that in this scheme the limiter restricts the overall order to second order and there is therefore little point in insisting on a third-order initial estimate for the gradient in the first step above. However this third-order scheme has the same computational cost as second order and is therefore commonly used instead. The van Leer limiter forces the method to be monotonicity preserving and prevents it from accentuating already existing extrema. It is therefore positivity preserving. This limiter has also been applied directly to the FB method; there is no significant difference between the results from such a scheme and those from VL and only the VL results are presented here. However, there are significant differences between the *basic*, i.e., without gradient limiters, FB method and those from VL and these will be highlighted in this paper.

2.3. Piecewise Parabolic Method (PPM)

As a next step in improving the accuracy of the scheme, the piecewise linear function used in FB and VL can be replaced by a piecewise parabolic function [10]:

- Compute a value for U at the cell boundaries (i.e., $U_{i+1/2}$ for each i) from a fourth-order interpolation scheme, which itself is limited to ensure that $U_{i+1/2} \in [U_i, U_{i+1}]$.
- Compute $\phi(y)$ on each cell as a parabolic function which passes through the previously calculated boundary values for each cell and which has the correct mean, i.e., $\int_{i-1/2}^{i+1/2} \phi(y)\, dy = U_i$.
- Apply a cellwise limiter to ϕ: if U_i is a local extremum, then set $\phi = U_i$ in the cell; if the interpolating parabola $\phi(y)$ achieves an extremum in the cell, then reset one of the boundary values (making ϕ discontinuous there) so that ϕ is then monotone and so that $d_y\phi = 0$ at the edge opposite to the resetting.

This method is monotonicity preserving and does not accentuate already existing extrema. For uniform grids, as used here, this scheme is formally third-order accurate away from extrema and first order at extrema. A variation of this method, which is used in some of the tests below, is to calculate $\Phi_{i+1/2}$ without applying limiters to ϕ. This is called the PPM1 scheme. A similar high-order geometric reconstruction has been used previously [5] but this was a third-order scheme and imposed positivity but not monotonicity.

2.4. Flux-Corrected Transport (FCT)

The flux-corrected transport algorithm [11] limits not the interpolating function ϕ but the resulting flux Φ:

- Update U_i by the first-order upwind method $\phi(y) = U_i$ for $i - 1/2 < y < i + 1/2$; call the result $\tilde{U}_i$. This method is well behaved but is very diffusive.
- Now compute the first-order upwind fluxes for $\tilde{U}_i$; call them $\Phi^{lo}_{i+1/2}$.
- Also compute fluxes for $\tilde{U}_i$ from a high-order method; call them $\Phi^{hi}_{i+1/2}$.
- Define the corrective flux

$$\Phi^c_{i+1/2} = s \max\big(0, \min\big[s(\tilde{U}_{i+2} - \tilde{U}_{i+1}), \big|\Phi^{hi}_{i+1/2} - \Phi^{lo}_{i+1/2}\big|, s(\tilde{U}_i - \tilde{U}_{i-1})\big]\big)$$

where $s = \text{sign}(\tilde{U}_{i+1} - \tilde{U}_i)$.

- Add the corrective antidiffusive flux $U^{n+1}_i = \tilde{U}_i - (\Phi^c_{i+1/2} - \Phi^c_{i-1/2})$.

The flux limiter allows the addition of as much antidiffusive flux as possible without breaking monotonicity preservation or allowing the accentuation of already existing extrema. In all of the tests below a fourth-order scheme has been used to calculate the high-order flux so that the FCT approach is formally of higher order than the PPM method for smooth, well-resolved functions. The FCT approach has been used previously in Vlasov simulations [12].

2.5. High-Order Compact Finite Difference (Compact)

As a higher order scheme we have tested a compact finite difference approach [13]. Here the time update is fourth-order Runge–Kutta with each intermediate step of the form $U^{n+1}_i = U^n_i + c\Delta t U'_i$. The local estimates of gradients U'_i are found from the sixth-order compact equation

$$\frac{1}{3}U'_{i-1} + U'_i + \frac{1}{3}U'_{i+1} = \frac{1}{36\Delta x}(U_{i-2} - 28U_{i-1} + 28U_{i+1} - U_{i+2}).$$

Fine-scale structures in the distribution functions are removed by applying a compact filter to the data after each time step of the form

$$\alpha U_{i-1} + U_i + \alpha U_{i+1} = a_0 U_i + a_1(U_{i-1} + U_{i+1}) + a_2(U_{i-2} + U_{i+2}) + a_3(U_{i-3} + U_{i+3}),$$

where $a_0 = (11 + 10\alpha)/16$, $a_1 = (15 + 34\alpha)/64$, $a_2 = (-3 + 6\alpha)/32$, $a_3 = (1 - 2\alpha)/64$, and throughout this paper $\alpha = 0.45$, where U_i are the new filtered values. This method does not maintain positivity or monotonicity. The motivation for testing a compact scheme comes from spectral transform methods for solving Vlasov's equation. The aim in this paper has been to focus on Eulerian fixed grids and thus the compact approach is chosen as the closest that grid-based methods can get to spectral accuracy. This approach can only remove fine-scale filamentation by filtering. The coefficients for the filter were found to be the best choice from the original work on compact schemes [13] for the problems tested.

3. THE TEST PROBLEMS

In all of the following tests we solve for the electron distribution function f_e, and where appropriate for the ion distribution function f_i, on an (x, v) grid with (N_x, N_v) equally spaced

points. The computational domain is defined in $0 < x < L_x$ with $-v_e^{\max} < v_e < v_e^{\max}$ for the electrons and $-v_i^{\max} < v_i < v_i^{\max}$ for the ions. Unless otherwise stated $v_i^{\max} = v_e^{\max}/M_r^{1/2}$, where the mass ratio $M_r = m_i/m_e$. All boundaries are taken to be periodic. This is not physically realistic for the velocity domain but $v_e^{\max}$ is always chosen to be sufficiently large that the boundaries in v-space do not influence the solution. Tests which do not solve for f_i assume a uniform background ion number density. Δt is fixed on each time step so that $\Delta t = \min(\Delta x/v_e^{\max}, \Delta v_e/|E|_{\max})$, where Δv_e is the grid spacing in the electron velocity. Since the advection sweeps are always with constant speed the CFL condition can be circumvented by first shifting the solution by an integer number of grid points and then using the algorithms described above for the remaining fractional step. This approach has not been used in any of the results in this paper, as it is the spatial accuracy of the schemes themselves which is being assessed.

3.1. Linear Landau Damping

This is the problem of the linear Landau damping of a Langmuir wave. The initial configuration is

$$f_e = (1 + \alpha \cos(kx)) \exp\left(-v_e^2/2\right)/\sqrt{2\pi},$$

where $\alpha = 0.01$, $L_x = 4\pi$, $v_e^{\max} = 4.5$, and $k = 0.5$. The ions are stationary. For these results we fix $N_x = 32$ and run tests with $N_v = 16$, 32, and 64. The solution directly obtained from the linear dispersion relation for this problem gives an oscillation frequency of $\omega = 1.41566$ and a damping rate of $\gamma = 0.153359$. Each test code is compared against these values by fitting a straight line across the maxima of $\log_e(E_1)$ vs t, where E_1 is the absolute value of the amplitude of the fundamental harmonic of the electric field. Figure 1 shows the evolution of $\log_e(E_1)$ for the codes `FB`, `Compact`, `FCT`, and `PPM` for $N_v = 64$. Note that the values of E_1 are from the unnormalized FFT routine and should be divided by $N_x/4$ to get the real

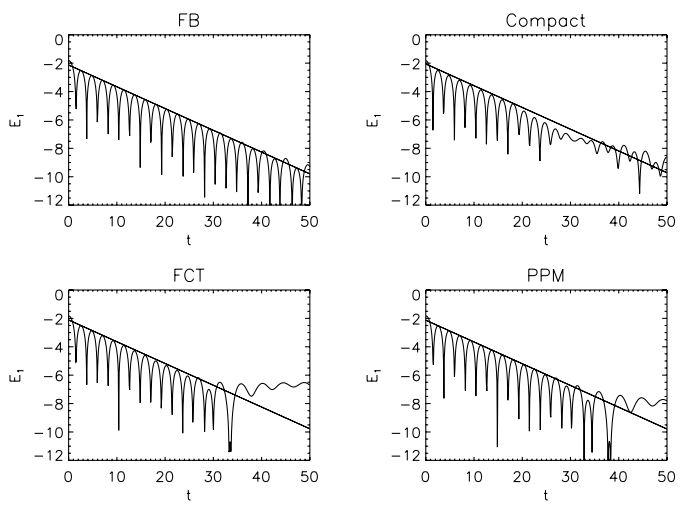

FIG. 1. Time evolution of the amplitude of the fundamental mode of the electric field for the linear Landau damping test with $(N_x, N_v) = (32, 64)$. The solid line represents the decay rate obtained directly from the linear dispersion relation.

TABLE I
Percentage Errors in the Damping Rate γ for Each Scheme for the Linear Landau Damping Test with $N_x = 32$

N_v	FB	VL	Compact	FCT	PPM	PPM1
16	16	15	47	70	4.7	3.7
32	2.6	1.6	3.3	10	2.2	0.038
64	0.32	6.0	5.1	28	1.7	0.13

amplitudes. However since it is only the gradient which is tested here this is unimportant. The results from the VL scheme are similar to those from the FB method and are not presented here. In each case the solid straight line is the analytic result for γ given above.

The percentage errors in ω and γ for each scheme on a variety of resolutions are shown in Table I. If the electric field is ignored in Vlasov's equation the solution is simply the free streaming of characteristics at the coordinate velocity v, different for each row in velocity space. After a time $T_R = 2\pi/(k\Delta v)$ each row in velocity space will be back in its initial condition. If the electric field is small and damped then there is a possibility that near T_R the solution will show signs of recurrence. For large initial E, or unstable modes in which E exponentially grows, this is not a problem but it is an issue for the Landau damping of small initial amplitude Langmuir modes. To avoid problems with the recurrence effect the best-fit line used to calculate the effective γ for each test was limited to only those maxima in E_1 which occur before $T_R/2$, and thus the time over which γ is estimated is different for each of the resolutions. Note that the analytic result for γ is only valid for late time. Thus both the early maxima and the deviation from linear decay before $T_R/2$ will contribute to the error estimates in Table I even though the early maxima are actually not necessarily in error when they differ from the fitted line. The same is also true of later times, as the linear theory of Landua damping breaks down before τ_b, the bounce time of trapped electrons. In this normalisation $\tau_b \simeq 2\pi/\alpha^{1/2}$ and thus $\tau_b \simeq 60$. For the highest resolution tested, i.e., $N_v = 64$, the upper limit of $t = T_R/2$ in estimating γ corresponds to $t = 44.7$. The poor performance of some schemes at higher resolution, e.g., the VL scheme being worse on higher resolutions, may therefore be due to the breakdown in the validity of the linear model used to estimate the percentage errors.

All of the codes (for the 32×32 resolution) conserve energy to within 0.01%. They also all conserve total mass to machine precision, and the largest total momentum recorded (which ought to be zero) for any of the simulations is 3×10^{-7}. So the disparity in the results presented in Table I is not due to a simple lack of conservation. Indeed, there are a number of features of the various codes which are highlighted by this test. These relate to the order of the schemes and the dissipation inherent in each approach.

Linear Landau damping is a useful test of Vlasov solvers, as the fine-scale structuring which is caused by phase mixing is known to generate a perturbed distribution function, f_1, which varies as $f_1 \sim \exp(ikvt)$. Hence for each v there will come a time when the perturbed distribution function has an effective wavelength of twice the grid spacing. For the FB method numerical dissipation would then be at its largest. Since the gradients are of $f_0 + f_1$, where f_0 is the equilibrium Maxwellian distribution, the gradients calculated are never large enough for f to become negative. This is shown below to be false for more stringent Vlasov test problems. Thus for linear Landau damping the numerical dissipation

inherent in the FB method is sufficient to thermalize the fine-scale structuring without introducing negative f. However, there is no guarantee that individual x or v direction advection sweeps are monotonicity preserving. These results show that this is not a major problem for the linear Landau test, as clearly the FB method gives an accurate result. Replacing the centered gradient used in FB with a van Leer-limited gradient has only a minor effect on the results, as can be seen from the VL results.

The results from the Compact code show that it is clearly worse than the lower order FB method. Since this is essentially a linear problem; one would normally expect higher order schemes to give more accurate results. However, there is less intrinsic dissipation in the Compact method and it therefore encounters problems when the fine-scale structuring approaches the grid size. At this stage the need to fit a high-order polynomial through rapidly oscillating values leads to large false gradients and these must be removed by the filtering. This filtering affects the linear properties of the damped mode, as can be seen at about $t = 20$ in Fig. 1. It is this which causes the averaged Landau decay rate to be inaccurate. The averaging used to find the damping rates in Table I will thus be different if averaged over $T_R/4$ instead of $T_R/2$. Using $T_R/2$ has the advantage that schemes which do not maintain linear decay for long enough lose out on this test. It may be possible to achieve better results for the Compact method by more carefully choosing the filtering scheme. Since the Compact method cannot be recommended for other reasons, which are outlined in the conclusions, we have not investigated this possibility further.

The FCT method gets the Landau decay correct initially but the limiters used in the algorithm prevent the fundamental from decaying after about $t = 30$ on the (32, 64) grid. Using the average over $T_R/2$ as the measure of accuracy, as in Table I, shows that the FCT limiters make this scheme the worst for the linear Landau problem.

By far the most accurate scheme is PPM1. This is a natural generalization of the FB method and it is not surprising therefore that it performs so well on this problem, bearing in mind the success of the FB method. As with FB the PPM1 scheme is accurate for this test but does not guarantee that individual x or v direction advection sweeps are monotonicity preserving. Including the standard monotonicity-preserving limiters gives the results presented for PPM. This limiting does degrade the accuracy of the scheme for this test but still gives results which are considerably more accurate than either the FCT or the Compact methods.

3.2. Bump-on-Tail Instability

This test studies the evolution of an unstable bump-on-tail electron distribution. The ions are stationary, $L_x = 2\pi/0.3$, $v_e^{\max} = 8$, and the initial electron distribution function is

$$f(x, v) = f_{b.o.t}(v)(1 + \alpha \cos(kx)),$$

where the bump-on-tail distribution is

$$f_{b.o.t}(v) = \frac{n_p}{\sqrt{2\pi}} \exp\left(-\frac{1}{2}v^2\right) + \frac{n_b}{\sqrt{2\pi}} \exp\left(-\frac{1}{2}\frac{(v - v_b)^2}{v_t^2}\right).$$

For these tests we take $n_p = 0.9$, $n_b = 0.2$, $v_b = 4.5$, $v_t = 0.5$, $\alpha = 0.04$, and $k = 0.3$. This distribution function is unstable and leads to a rapid increase in the electric field. As all of the schemes have dissipation of some sort (implicit for FB, filtering for Compact, and primarily through limiters for FCT and PPM) the system will eventually damp the fine-scale structures

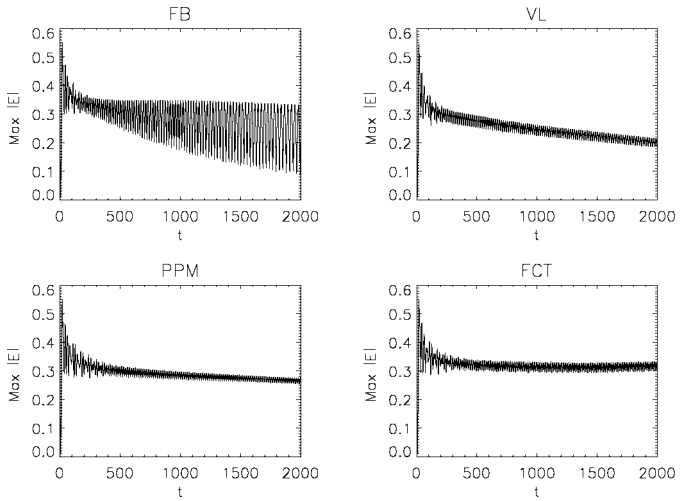

FIG. 2. Time evolution of $|E|_{\max}$ for the bump-on-tail test on a (128, 128) grid.

and be attracted to a stable BGK mode. Before considering the structure of the BGK mode formed by each scheme, it is worth looking closely at the evolution of the maximum value of the absolute magnitude of the electric field, $|E|_{\max}$, against time. Figure 2 show the evolution of $|E|_{\max}$ for four schemes with a resolution of $(N_x, N_v) = (128, 128)$.

The result from the FB code stands out as clearly in error. This is confirmed in Fig. 3, where these tests are repeated with a (512, 512) grid for the FB and PPM methods. This verifies that the results obtained on a (128, 128) grid for the high-order limited schemes are indeed reliable.

When a van Leer-limited gradient is added to the FB method, i.e., the VL code, the false large oscillations in $|E|_{\max}$ are removed, as can be seen from the plot in Fig. 2. Since this scheme is formally lower order than either the FCT or PPM method the mean value of $|E|_{\max}$ is dissipated more quickly. Results from the Compact scheme are similar to those already presented for the PPM scheme.

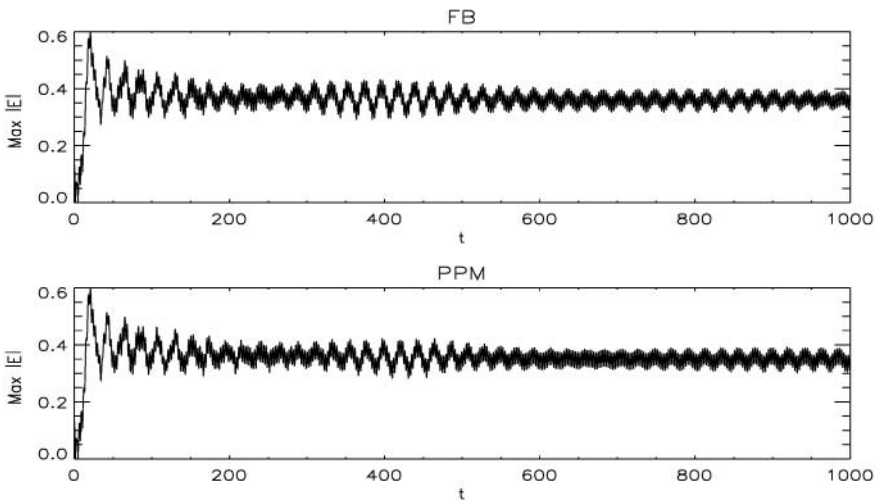

FIG. 3. Time evolution of $|E|_{\max}$ for the bump-on-tail test on a (512, 512) grid.

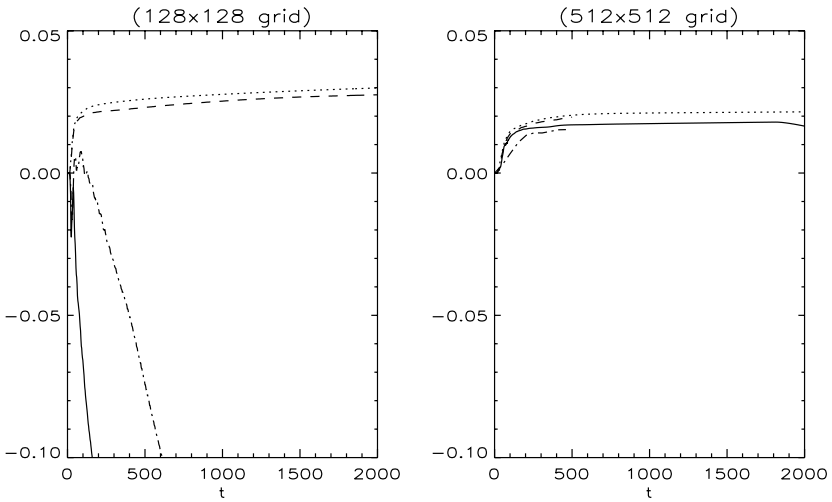

FIG. 4. Time evolution of the fractional change in discrete kinetic entropy for the bump-on-tail test with resolution (128, 128) and (512, 512). The solid line is for FB, the dotted line is PPM, the dashed line is FCT, and the dash–dotted line is Compact.

Now that the distribution function can contain large gradients and complex structures (unlike the linear Landau damping test) the lack of monotonicity and positivity is more significant. To quantify this, Fig. 4 shows the evolution of the fractional change in the discrete kinetic entropy, $S(t)$, for some of the schemes on (128, 128) and (512, 512) grids. Here $S(t) = -\sum f_i \log_e(g_i)$, where the sum is over all points on the computational grid and $g_i = \max(f_i, 10^{-64})$ is used to avoid taking the logarithm of negative f. Plotted in Fig. 4 is the fractional change $\delta S = (S(t) - S(0))/S(0)$. On the (128, 128) grid both the FB and Compact schemes immediately lead to a decrease in $S(t)$. The scale has been chosen to allow easy comparison between schemes and resolutions so the FB and Compact lines on the (128, 128) grid actually go off the bottom of the scale. They continue to decrease approximately linearly for the duration of the simulation, although this is not shown. It is therefore not simply the lack of positivity which is responsible for the oscillation in $|E|_{\max}$ growing for the FB method in Fig. 2, as the Compact scheme also has regions of negative f but does not show signs of growth in the oscillations of $|E|_{\max}$. Also fixing the lack of monotonicity in the FB approach with van Leer limiters removes the growth in $|E|_{\max}$ and makes $S(t)$ monotonically increasing. The problems inherent in the FB method therefore do not stem from the formal order of the scheme but must result from an incorrect handling of short scale lengths. Since FB performs well on a (512, 512) grid it seems likely that for this particular test problem there is a critical scale length which must be handled correctly, i.e., without introducing false maxima and minima, before reliable answers are obtained. All of the limited schemes automatically guarantee that they do not introduce false extrema, irrespective of the resolution, show no growth of $|E|_{\max}$, and only have increasing kinetic entropy.

In order to quantify the results from the bump-on-tail test problem we have run the PPM, FCT, Compact, FB, and VL codes on a (512, 512) grid up to $t = 500$ and then for each of the schemes calculated $\bar{f}(v_j) = \sum_i f(x_i, v_j)/N_x$. To remove any biasing in the solutions the average of this over all schemes is taken to be the accurate solution, $\bar{f}^{\text{acc}}$, and this is then used to find the L_1 norm of the error for each of the schemes on lower resolutions, where $L_1 = \sum_j |\bar{f}(v_j) - \bar{f}^{\text{acc}}(v_j)|/N_v$.

TABLE II
L_1 Errors for Each Scheme for the Bump-on-Tail Test

(N_x, N_v)	Compact	PPM	FCT	FB	VL
(32, 32)	0.017	0.010	0.0072	0.030	0.018
(64, 64)	0.0025	0.0049	0.0036	0.014	0.011
(128, 128)	0.00060	0.0016	0.0011	0.0038	0.0033
(512, 512)	0.00052	0.00039	0.00033	0.00058	0.00026

The results of this analysis are shown in Table II, which includes the results on the (512, 512) grid to show that all codes converge to the same answer and that the L_1 norm estimates for courser grids are not biased strongly by a lack of convergence. However the result for the Compact scheme on a (128, 128) grid is too close to the variance in the results used to find $\bar{f}^{\text{acc}}$ to be used as anything other than a rough estimate. These results confirm that the FCT and PPM methods are of about the same accuracy as are the FB and VL methods. However, unlike the linear Landau damping test the results here follow the formal accuracy of the schemes, with the best results being from the higher order schemes and the low-order schemes (FB and VL) being more diffusive. This can be seen clearly in Fig. 5. However, it should be remembered that while the Compact scheme gives accurate results based on the L_1 norm of the error it gives poor results if the kinetic entropy is used as the measure of accuracy.

Shaded surface plots of f are also useful in determining the properties of these schemes. Figure 6 shows such plots, on a (512, 512) grid, for the whole x domain but is restricted to $v_e > 0$, as this is the side in which a BGK mode forms. All of the schemes are broadly similar except for two notable features. First, the BGK mode phase space hole is not in the same place in the FB method as in the others. This is not purely an effect of the order of the schemes, as the VL method does not agree with the FB method. The second important point is that the higher order schemes do, as expected, show more detail in the vicinity of the hole. However, while the PPM method has a smooth solution the FCT solution shows signs

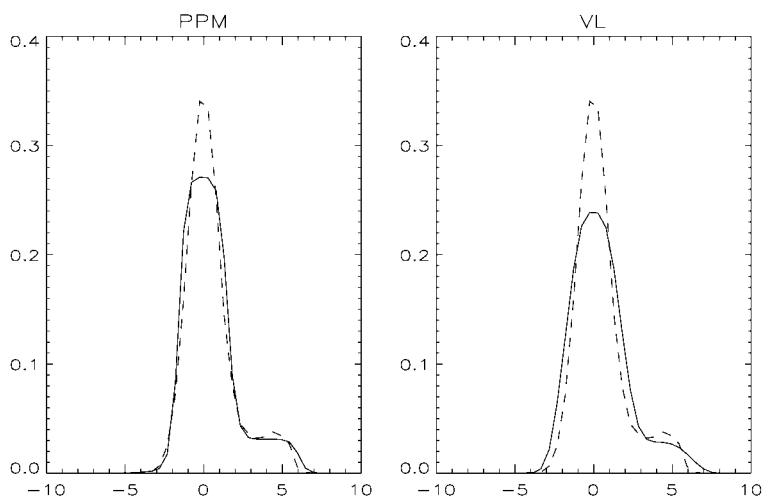

FIG. 5. Spatially averaged $\bar{f}$ for the PPM and VL methods. The dashed line is $\bar{f}^{\text{acc}}$ defined from an average of the (512, 512) grid results and the solid lines are the results from the (32, 32) grids.

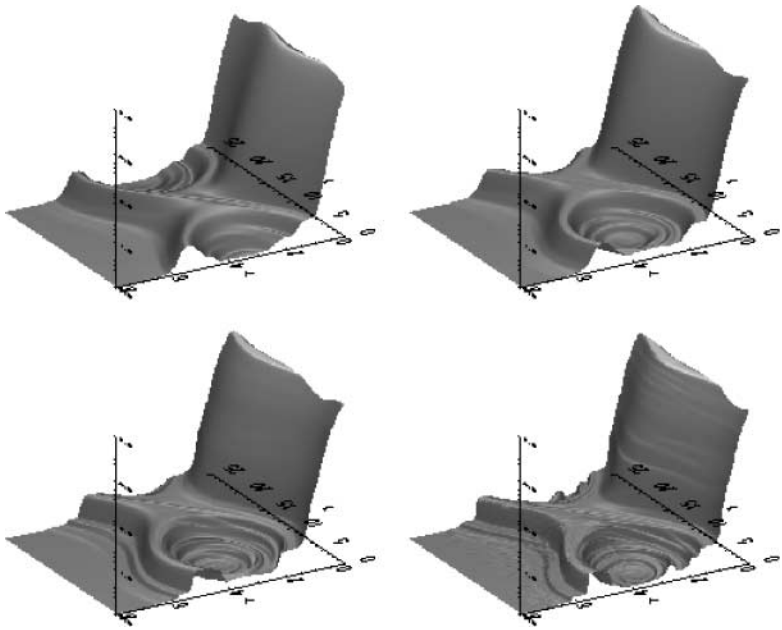

FIG. 6. Bump-on-tail phase space holes at $t = 500$ with a (512, 512) grid for the FB (top left), VL (top right), PPM (bottom left), and FCT (bottom right) methods. Shown are shaded surfaces of f for the whole of x but with only $0 < v_e < 8$.

of terracing. This well-known problem with FCT approaches is discussed in more detail in the next section.

On lower resolutions the advantages of the PPM method are more apparent, as can be seen in Fig. 7, which compares it to the VL method on a (64, 64) grid. This is a demonstration of the kind of accuracy one would expect when resolving small-scale structures on more complex problems.

3.3. Ion-Acoustic Turbulence

Here the motivation is to compare the results from the different schemes not for a single well-defined mode but for a turbulent spectrum. The problem chosen is the onset and saturation of the ion-acoustic instability. The initial conditions are $L_x = 2\pi/0.05$, $v_e^{\max} = 8$,

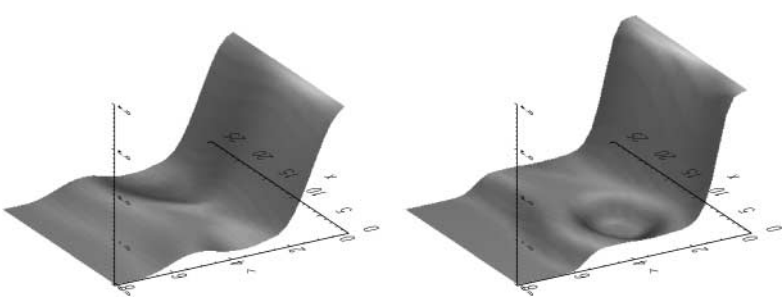

FIG. 7. Repeat of Fig. 6 on a (64, 64) grid for the VL (left) and PPM (right) methods.

$M_r = 1000$, and the ion distribution function is defined at all spatial grid points to be

$$f_i = \left(\frac{M_r}{2\pi}\right)^{1/2} \exp\left(-\frac{M_r}{2} v_i^2\right).$$

The electrons are set up as a drifting Maxwellian such that

$$f_e = (1 + a(x))\left(\frac{1}{\sqrt{2\pi}}\right) \exp\left(-\frac{1}{2}(v_e - U_e)^2\right),$$

where $U_e = -2$ and

$$a(x) = 0.01(\sin(x) + \sin(0.5x) + \sin(0.1x) + \sin(0.15x) + \sin(0.2x) + \cos(0.25x) + \cos(0.3x) + \cos(0.35x)).$$

The intention here is to provide initial conditions which are clear and allow others to repeat the tests using other codes should they wish to do so. This motivated the choice of $a(x)$ to be fixed and not a low-level random noise.

This choice of initial conditions leads to an unstable growth of ion-acoustic waves. The electric field fluctuations which are established lead to a transfer of momentum from the electrons to the ions. This is seen in a plot of the difference of ion and electron fluid speeds, u_i, and u_e, respectively, in Fig. 8. On the higher resolution tests all schemes agree on the decay rate. On the lower resolution tests there is a clear discrepancy in the time of onset of the decay. In this regard the PPM and FCT methods are more accurate since the higher order approach more accurately resolves the linearly unstable ion-acoustic modes and thus the initial growth of the fluctuating electric field responsible for the momentum transfer. Estimating the asymptotic value of $|u_i - u_e|$ from the (512, 512) results alone is not helpful

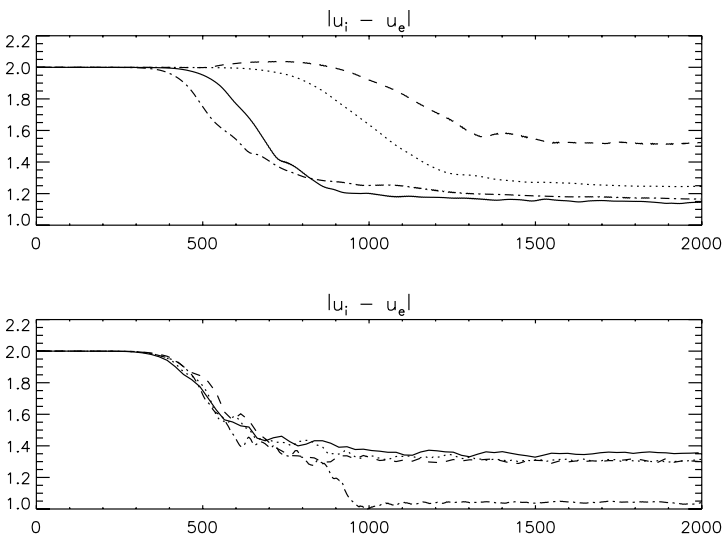

FIG. 8. Evolution of the $|u_i - u_e|$ for the PPM, FB, VL, and FCT schemes on two resolutions. In both plots the solid lines are PPM, the dotted lines are VL, the dashed lines are FB, and the dot–dashed lines are FCT. The upper figure is on a (64, 64) grid and the lower figure is on (512, 512).

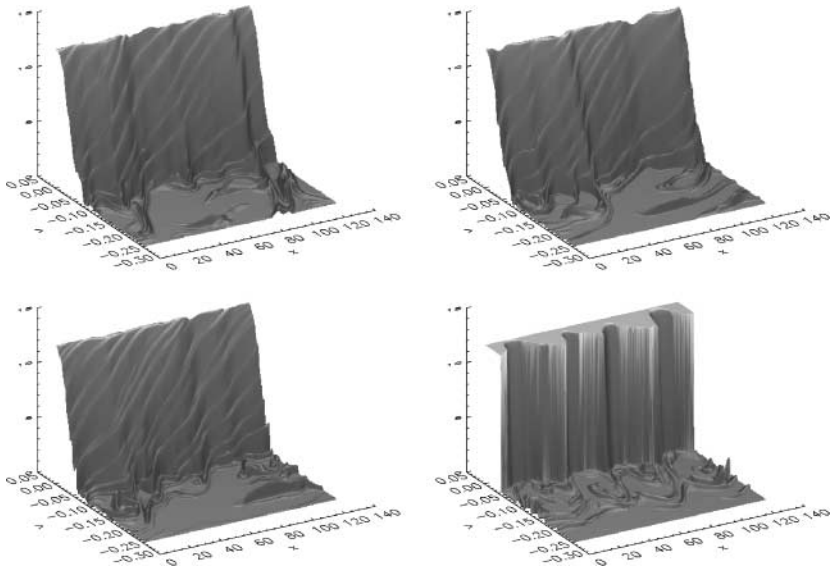

FIG. 9. Ion-acoustic turbulence test at $t = 2000$ with a (512, 512) grid for the FB (top left), VL (top right), PPM (bottom left), and FCT (bottom right) methods. Shown are shaded surfaces of f_i for the whole of x but with only $-8 < v_i < 0$.

due to the low value predicted by the FCT scheme. However, we can rule out the FCT result by looking at shaded surface plots of f_i at $t = 2000$ in Fig. 9. These show f_i in the whole of the x domain but only $v_i < 0$. Clearly from these plots the FCT scheme has clipped the maximum severely and similar plots of f_e show that the terracing, already hinted at in Fig. 6, is now far more pronounced. We use these facts to rule out the high-resolution FCT results and conclude that the estimated final value of $|u_i - u_e|$ is 1.35, from the average of the PPM and VL results. On the (64, 64) grid results of Fig. 8 there is little difference in the accuracy of the FB and PPM in estimating the asymptotic value of $|u_i - u_e|$. PPM is, however, more accurate in determining the time dependence of $|u_i - u_e|$.

4. SOLVING AMPÈRE INSTEAD OF POISSON

There has been some interest in developing codes that solve Ampère's equation instead of Poisson's equation [4] since using Ampère's equation leads to a scheme that is easier to parallelize efficiently. We note, however, that using Ampère's equation may introduce a systematic error into the electric field which might significantly change the results. It is therefore important to check that the results we obtain are independent of whichever of the two equations we use to close the system algebraically. Here we make a comparison by considering the bump-on-tail example, with one species, using the PPM method on a (128, 128) grid up to $t = 2000$, but using the following time-stepping method:

- Evolve $\partial_t f + v\partial_x f = 0$ for a time $\Delta t/2$.
- Solve $\partial_t E = \int v(f - \bar{f})\, dv$ for a time $\Delta t/2$.
- Evolve $\partial_t f + E\partial_v f = 0$ for a time Δt.
- Again solve $\partial_t E = \int v(f - \bar{f})\, dv$ for a time $\Delta t/2$.
- Finally, evolve $\partial_t f + v\partial_x f = 0$ for a time $\Delta t/2$.

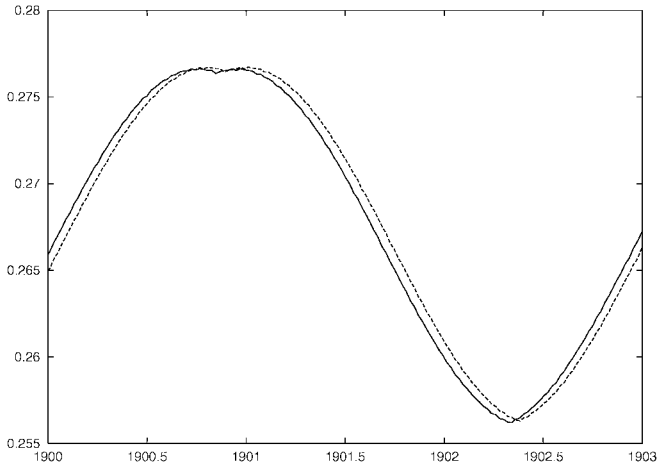

FIG. 10. $|E|_{\max}$ vs time for the bump-on-tail example. The solid line is from the method used when comparing the various advection algorithms; the dashed line solves Ampère's equation. We note that the only discernible difference is a time shift of about 1% of a plasma oscillation period.

At each time step, we compare the fundamental component of the electric field obtained from Ampère's equation to the value computed from Poisson's equation for the system at that time. The relative error in $|E_1|$ is always less than 0.15% and the phase error is always less than 0.001 radians. In Fig. 10, we have plotted $|E|_{\max}$ against $t \in [1900, 1903]$ both for the time-stepping method given here and for the time-stepping method used in the comparison of the different advection algorithms. We note that there is a time shift of 0.05, which corresponds to approximately 1% of the period of a plasma oscillation. We conclude that there is no significant loss of accuracy. However, for electrostatic problems one should still of course check the accuracy against Poisson as a diagnostic.

5. CONCLUSIONS

This paper has presented a series of test problems for conservatively differenced, fixed Eulerian-grid-based Vlasov solvers. All of the codes have adopted the dimensional splitting approach as introduced by Cheng and Knorr [3]. This is an efficient mechanism for solving Vlasov problems, as each of the spatial and velocity advection sweeps are at constant speed. The central issue is then how best to solve for each of these 1D steps. What qualifies as a "best" technique is not, however, a straightforward question when dealing with Vlasov solvers. Ideally any Vlasov solver should maintain positivity; actually the solution is bounded for all time by the initial maximum and minimum of f, and the advection steps should be monotonicity preserving. Determining how important these two conditions are in a quantifiable way for these test problems is a central focus of this work. The other major concern of this paper has been the treatment of the fine-scale structure in f which arises naturally in many Vlasov problems. Treatment of the fine scales (actually their averaging, smoothing, or filtering) is intimately related to maintaining monotonicity.

Using Cheng and Knorr's [3] time-splitting scheme as a common template for all of the tests allows us to isolate issues of performance and accuracy solely to the choice of advection algorithm. We have compared second-order spatially accurate schemes (`FB` and `VL`),

third/fourth-order schemes (PPM and FCT), and a sixth-order compact scheme (Compact). Some of these maintain monotonicity and positivity by geometrical construction (VL and PPM) while others achieve this by flux limiting (FCT). The schemes which are not positivity or monotonicity preserving (FB and Compact) must use filtering or smoothing to remove fine-scale structures. This has been applied in the Compact scheme, which fails all of the tests without it, but not to the FB method. However the FB method does work, even without smoothing, on some of the problems and gives some useful insight into the numerical problems associated with Vlasov solvers. If the FB method were to be used for Vlasov research it must of course be coupled with smoothing, as for example in [8].

The test problems were chosen to represent the most common applications of Vlasov solvers. The Landau problem tests the ability to deal with linear problems. The bump-on tail test highlights accuracy of the different codes in dealing with a single unstable mode and the formation of a stable BGK mode. Finally the ion-acoustic turbulence test was used to compare the codes when the physics was being driven by a broad spectrum of unstable modes. In all these tests it is also important to measure the relative costs of the numerical schemes. For 100 steps on the (512, 512) grid bump-on-tail problem the run times were as follows: FB, 8 s; VL, 14 s; PPM, 19 s; and Compact, 164 s. These timings were on a Compaq EV6 500-Mhz CPU with 4-MB cache using the Compaq F90 compiler. As always with such comparisons one needs to be cautious that such scalings will remain true on all architectures but the general picture is probably reliable. The fastest is the FB method without smoothing or averaging. Adding limiters to the FB method (it does not work for all problems on all grid sizes without this) approximately doubles the run time. Going from second-order VL to third-order PPM increases the run time by about 35% and the Compact scheme is almost an order of magnitude slower.

The linear Landau test showed that all schemes get a reasonably accurate decay of the fundamental mode. The percentage errors in Table I are mostly dominated by the departure from exponential decay at later times. The FB and Compact schemes maintain the decay, although in the Compact solution the filtering required for this scheme to work changes the decay rate at around $t = 25$. Both the PPM and FCT schemes give an accurate initial decay but then maintain an approximately constant level for $|E_1|$ until T_R. However, since $|E_1|$ has decreased by about three orders of magnitude before this happens, i.e., $|E_1| \simeq 10^{-5}$, this is not seen as a major drawback for practical situations.

The bump-on-tail test showed the problem of using schemes of second order or higher which do not correctly handle the fine-scale structures. Here the FB method fails on a (128, 128) grid, as can be seen in Fig. 2. Some evidence that it is the handling of these fine scales that is most important, in contrast to merely maintaining positivity, is given by the results from the Compact scheme. This also has regions with $f < 0$ (see Fig. 4), but in all other quantifiable ways gives a satisfactory result. The same is true of the FB method when suitable smoothing is included [8]. The remainder of the results in Section 3.2 emphasize the advantages of going to higher order schemes, with the VL method needing approximately double the number of points in x and v to achieve the same detail in the structure of the BGK mode as the PPM method.

The final test reemphasized the advantages of using higher order schemes in getting accurate results for $|u_i - u_e|$ as a function of time. More important, this test showed that the FCT approach actually gives the wrong answer due to excessive clipping of the maxima of f_i and terracing of f_e. Hence maintaining positivity and monotonicity by themselves is not sufficient to guarantee an accurate solution. It is vital that the limiter, or indeed smoother,

and so forth, for the FB method and variants dissipates the fine-scale structure in a physically realistic way. This is true of the PPM method and the filtering in Compact.

From all of these observations and results we draw the following conclusions:

- Applying geometric limiters to the FB method, i.e., VL, maintains positivity and monotonicity and removes the need for additional smoothing or averaging.
- The PPM method, which also needs no additional averaging, is approximately 35% slower than VL but gives results which are quantitatively more accurate.
- The FCT approach fails on the ion-acoustic test due to excessive clipping and terracing and therefore cannot be recommended as a method for solving Vlasov problems.
- The Compact method is the most accurate on the bump-on-tail test when using the L_1 norm of the error as the measure of accuracy. However it does not maintain $f > 0$, has very poor entropy results on course grids, and is approximately an order of magnitude slower than PPM.
- Keeping $f > 0$, while desirable, is less important than correctly treating the fine-scale structures which form in Vlasov solutions.

Since maintaining monotonicity and positivity is a property of linear advection and implementing it in Vlasov solvers removes the need for additional averaging or smoothing the optimal scheme from these tests is the PPM method. It consistently gives accurate results (it is formally third-order accurate) and is only 35% slower than VL. It is over two times slower than FB but comparison with VL is more appropriate, as the FB method needs additional smoothing to be reliable, which would of course slow it down. For VL to achieve the same resolution of phase space as PPM it requires double the number of points in x and v, which increases the VL run time by a factor of eight. A similar conclusion was reached previously by Filbet *et al.* [5] regarding the benefits of higher order geometric reconstructions. However, in that paper, Filbet *et al.* consider only third-order reconstructions and the limiters applied maintain positivity but not monotonicity. The results presented in this paper are the first to implement the full PPM algorithm to Vlasov solvers and demonstrate the robustness and accuracy of such an approach.

The high-order compact scheme is the most accurate in the L_1-norm analysis of the bump-on-tail problem. However, as has already been mentioned, this scheme only works with compact filtering of the fine-scale structures. Compact also requires more memory, as it is only stable with third, or higher, order Runge–Kutta, which requires extra temporary arrays. All of the other schemes, including PPM, require storage only for f_e and f_i so it is hard to recommend Compact despite its increased accuracy for the bump-on-tail test. Note also that the filtering made Compact less accurate than PPM for the Landau test. The fact that filtering in this way does work, although allowing $f < 0$ raises important questions about applying filtering or smoothing to Vlasov solvers. It may be possible to choose a filtering which improves further the accuracy of Compact. We have not attempted this, as the run time and memory costs make Compact impractical. Considerable effort has in the past been applied to the filtering/smoothing problem of other schemes. Most noticeable amongst these is the filtering technique first introduced by Klimas [14], which has the advantage of correctly evolving the fields, i.e., low-order moments are correct, by solving directly for the smoothed/filtered distribution function. This approach has only been shown to work in Fourier–Fourier transform space and thus does have the disadvantage of requiring multiple FFTs per step. We have concentrated on fixed Eulerian-grid-based solvers, and the merits of the PPM method compared to a suitably filtered Fourier–Fourier transform space solver

remain an open question. A physically and mathematically justifiable approach, such as the PPM geometric reconstruction, is successful in treating fine scales, automatically maintains positivity and monotonicity, and requires no additional smoothing. Unless a scheme which employs smoothing/filtering can be shown to be more accurate than this third-order approach it is difficult to see a strong case for using filtering on fixed Eulerian grid Vlasov solvers. Such techniques will, however, continue to be vital for semi-Lagrangian methods where 2D generalizations of a dimensionally unsplit PPM method would be cumbersome. We do, however, note that the third-order positive, but not monotonicity preserving, scheme used by Filbet *et al.* [5] has already been shown to be almost as accurate as cubic spline semi-Lagrangian methods anyway. There is therefore a very strong case for the third-order-accurate, positivity and monotonicity preserving PPM method proposed in this paper.

ACKNOWLEDGMENT

R. Vann was supported by an EPSRC and Euratom/UKAEA CASE award while working on this paper.

REFERENCES

1. H. X. Vu, D. F. DuBois, and B. Bezzerides, Transient enhancement and detuning of laser-driven parametric instabilities by particle trapping, *Phys. Rev. Lett.* **86**, 4306 (2001).
2. P. Birch and S. C. Chapman, Detailed structure and dynamics in particle-in-cell simulations of the lunar wake, *Phys. Plasma* **8**, 4551 (2001).
3. C. Z. Cheng and G. Knorr, The integration of the Vlasov equation in configuration space, *J. Comput. Phys.* **22**, 330 (1976).
4. R. B. Horne and M. P. Freeman, A new code for electrostatic simulation by numerical integration of the Vlasov and Ampère's equations using MacCormack's method, *J. Comput. Phys.* **171**, 182 (2001).
5. F. Filbet, E. Sonnendrücker, and P. Bertrand, Conservative numerical schemes for the Vlasov equation, *J. Comput. Phys.* **172**, 166 (2001).
6. T. P. Armstrong, R. C. Harding, G. Knorr, and D. Montgomery, Solution of Vlasov's equation by transform methods, in *Advances in Computational Physics* (Academic Press, San Diego, 1976), Vol. 9, p. 29.
7. E. Sonnendrücker, J. Roche, P. Bertrand, and A. Ghizzo, The semi-Lagrangian method for the numerical resolution of the Vlasov equation, *J. Comput. Phys.* **149**, 201 (1999).
8. E. Fijalkow, A numerical solution to the Vlasov equation, *Comput. Phys. Commun.* **116**, 319 (1999).
9. D. L. Youngs, Time dependent multi-material flow with large fluid distortion, in *Numerical Methods in Fluid Dynamics*, edited by K. W. Morton and M. J. Baines (Academic Press, New York, 1982), p. 273.
10. P. Colella and P. R. Woodward, The piecewise parabolic method (PPM) for gas-dynamical simulations, *J. Comput. Phys.* **54**, 174 (1984).
11. J. P. Boris and D. L. Book, Flux-corrected transport. I: SHASTA—a fluid transport algorithm that really works, *J. Comput. Phys.* **11**, 38 (1973).
12. K. Theilhaber, G. Laval, and D. Pesme, Numerical simulations of turbulent trapping in the weak beam-plasma instability, *Phys. Fluids* **30**, 3129 (1987).
13. S. K. Lele, Compact finite difference schemes with spectral-like accuracy, *J. Comput. Phys.* **103**, 16 (1992).
14. A. J. Klimas, A method for overcoming the velocity space filamentation problem in collisionless plasma model solutions, *J. Comput. Phys.* **68**, 202 (1987).